The ALPS II Experiment
Status Report to the DESY PRC

The ALPS II Collaboration:
Albert-Einstein-Institute, Hanover, Germany
DESY in Hamburg, Germany
Johannes Gutenberg-University Mainz, Germany
University of Florida, Gainesville, USA
University of Hamburg, Germany

March 7, 2017

Contents

1 Summary

Since the last meeting of the PRC the physics case for ALPS II has not changed. Still our understanding of the universe's transparency to TeV photons and of stellar cooling is challenged and still axions or axion-like particles remain a plausible explanation for the discrepancies between data and theory. Lots of activities in theory are taking place at present concerning dark matter axions and ALPs, which are however out of reach for ALPS II.

At ALPS IIa again important milestones concerning the optics development have been reached. The 10 m long regeneration cavity has been set up and characterized. A power built-up factor of 14,000 ± 3,000 corresponding to intra-cavity losses of 55±7 ppm has been demonstrated.. To reach the final specifications these losses are to be reduced to about 20 ppm.

A fist version of the central breadboard (hosting the flat mirrors defining the optical axes of the production and regeneration cavities) was installed at the ALPS IIa laboratory. The relative positioning of both mirrors has been proven to be stable in time and first results indicate well aligned optical axes of both cavities. The next important steps include establishing a simultaneous lock of the regeneration cavity to 1064 and 532 nm light, a lock of this cavity by controlling its lengths and investigating further the thermal effects observed in the production cavity.

The collaboration is also discussing a revised optical concept to benefit from lessons learned at ALPS IIa and to allow for simpler switching between the two detector systems.

For the detection system based on the Transitions Edge Senor (TES) the problems of the ADR cryostat as lined out in our last PRC report could not be solved. It was therefore decided to purchase a new dilution refrigerator thanks to extra funding from DESY. The tendering procedure is just ongoing and we hope to have a new system running in autumn to continue the TES studies. In between a new concept to suppress black-body induced background on the TES (the largest source of "dark counts") has been developed and will be tested in the next months. We are confident to be able to diminish this background to a negligible level.

For the heterodyne detection scheme, first encouraging results have been achieved at the University of Florida. In the near future this scheme will be tested with low "signal" fluxes.

Previously we had foreseen a data run at ALPS IIa searching for hidden photons in 2017. Due to the problems with the TES cryostat we most likely have to delay this to the year 2018. Otherwise the overall schedule for the project remains largely unchanged at present. Intense discussion with the DESY technical infrastructure groups on ALPS IIc have stated. We hope to begin with clearing the HERA tunnel in the North area in spring this year. At the same time HERA dipole straightening, which is on the critical path at present, should resume. By summer 2017 a more binding time schedule for installing ALPS IIc in HERA should be agreed on.

2 Reply to the questions and recommendations by the PRC

Here we reply to the risks and recommendations as given by the PRC after its October 2016 meeting.

Technical risks

1. *Dirt or other debris in the magnet bore (dust etc.) will not allow power build-up in the cavity. When next a magnet is cooled, a dust study could be done.*
   We did cleaning studies before at the ALPS IIa site. ALPS IIa is operated with old accelerator vacuum tubes which had to be cleaned extensively in 2012 by us. At present it seems that the extra losses in the cavity are caused by some micro-roughness of the mirror substrates.

2. *Problems with the TES/cryostat. This risk would disappear with a heterodyne / homodyne detector, but the latter set-up needs more R&D.*
   We are in the process of purchasing a dilution refrigerator thanks to extra ALPS funding provided by DESY. We would like to stick to the approach of having two different detection techniques at ALPS II.

3. *Vibrations and seismic noise. It may be that ground or magnet vibrations couple into the optical vacuum system and into the optics. When next a magnet is cooled, the vibration could be studied. Also, the acceptable ground-motion envelope is not yet calculated and the full ground-motion spectrum not yet measured. It may be that a more aggressive optics-table isolation is needed, perhaps a suspension from the vacuum tank as mentioned by the group. In order not to delay the vacuum-tank specification, this vibration-isolation design needs to be done by perhaps late 2017.*
   From our operation and in-depth study of the production cavity at the ALPS IIa site we think we have a clear understanding of the seismic isolation requirements. We have also compared the seismic noise at the ALPS IIa site with own measurements and archival data of the seismic noise in the HERA tunnel where ALPS IIc is to be constructed. No significant differences have been found. Still missing are studies in the HERA tunnel on long term (seasonal) drifts between HERA hall and tunnel. The production cavity studies have shown that locking the laser frequency to the cavity length fluctuations easily copes with the seismic noise.
   We have started to design seismic noise insulation design with a dedicated Ph.D. in engineering last year. However, recent studies of length lock techniques might indicate that we do not need much advanced isolation at ALPS IIa. We aim for clarifying this with dedicated measurements in April this year.
   We have not studied yet possible additional vibrations caused by magnet cooling.

Due to the priority of XFEL work on the HERA dipoles has not been re-started yet.

Program risks

1. *Lack of personnel, especially integration engineer and suitable and timely replacement for post-docs with optical expertise.*
   Both issues are under discussion with the FH management. A solution concerning the integration engineering is indicated for summer 2017, but the optical expertise at DESY is still a project risk. The two experts at work have DESY-contracts up to the end of 2018 and mid of 2020 respectively. However, the collaboration cannot expect both staying at DESY up to the end of their contracts, because both have to plan (and do so) for next steps in their career.

2. *X-FEL related delays.*
   At present the XFEL commissioning proceeds smoothly.

Recommendations for ALPS

- *Continue project discussion with DESY management: come to closure on the ALPSII project issue.*
  We are working on the formal project proposal, but still a thorough review of the HERA tunnel and hall infrastructure by the corresponding DESY experts has to take place.

- *Develop DESY personnel-task milestones (especially tunnel clearing and magnets). Link this to the project critical path. Get commitments for those personnel resources on that timeline.*
  A detailed project plan for the work in the tunnel has been set up and discussed with the corresponding infrastructure groups at DESY. The critical path is still given by the magnet straightening timeline.
  Previous agreements on available personal resources for clearing the HERA tunnel and setting up the magnet string had to be modified. Now extra personnel are to be financed by ALPS, corresponding funds need to be identified.
  A similar situation has emerged at the DESY mechanical workshop concerning the production of the components to straighten the HERA dipoles.

- *Check if the present postdoc optics personnel is sufficient. As those postdocs leave, plan to transfer their expertise to new postdocs. Since this expertise is vital to the project maybe a more efficient hiring scheme for postdocs targeted to fellows with optical experience should be considered.*
  At present the two optics postdocs do a great job, but please see our comments above. It remains challenging to attract optics experts for a particle physics fellowship at DESY.

- *The need for an engineer for tunnel integration is serious and needs a discussion with lab management.*
  As also mentioned above already we might find a solution in summer 2017.

3 Phenomenology of WISPs

3.1 Redefining the Axion Window

In Ref. [**?**] precise phenomenological requirements were formulated in order to define the parameter region of realistic axion models. The authors consisered KSVZ-type hadronic axion models and classified the representations R_Q of the new heavy quarks Q. By requiring that *i*) the Q are sufficiently short lived to avoid issues with long lived strongly interacting relics, *ii*) no Landau poles are induced below the Planck scale, fifteen cases were selected, which define a phenomenologically preferred axion window bounded by a maximum (minimum) value of the axion-photon coupling about twice (four times) larger than commonly assumed, cf. Fig. 3.1 (left). Allowing for more than one R_Q, larger couplings, as well as complete axion-photon decoupling, become possible.

3.2 The photo-philic QCD axion

Based on the "clockwork" mechanism, a framework was proposed in which the QCD axion has an exponentially large coupling to photons [**?**]. It opens new discovery space for the QCD axion outside the usual axion band as can be inferred from Fig. 3.1 (right). Importantly, in addition to the axion, the model predicts a large number of pseudoscalars which can be light and observable at the LHC. In the most favorable scenario, axion dark matter will give a signal in multiple axion detection experiments and the pseudo-scalars will be discovered at the LHC, allowing then to determine most of the parameters of the model.

3.3 The ALP miracle: unified inflaton and dark matter

In Ref. [**?**], a scenario was proposed in which both inflation and dark matter are described by a single axion-like particle (ALP) in a unified manner. It exploits minimal axion hilltop inflation, in which the effective masses at the maximum and mimimum of the potential have equal magnitude but opposite sign. Correspondingly, the ALP inflaton is light both during inflation and in the true vacuum. After inflation, most of the ALPs decay and evaporate into plasma through their coupling to photons, and the remaining ones become dark matter. The authors find that the observed CMB and matter power spectrum as well as the dark matter abundance point to an ALP of mass $m_a = \mathcal{O}(0.01)\,\mathrm{eV}$ and the axion-photon coupling $g_{a\gamma\gamma} = \mathcal{O}(10^{-11})\,\mathrm{GeV}^{-1}$: *the ALP miracle.* The suggested parameter region is within the reach of the next generation axion helioscope, IAXO, see Fig. 3.2 (left). Furthermore, thermalized ALPs contribute to hot dark matter and its abundance is given in terms of the effective number of extra neutrino species, $\Delta N_{\mathrm{eff}} \simeq 0.03$, which can be tested by future CMB experiments.

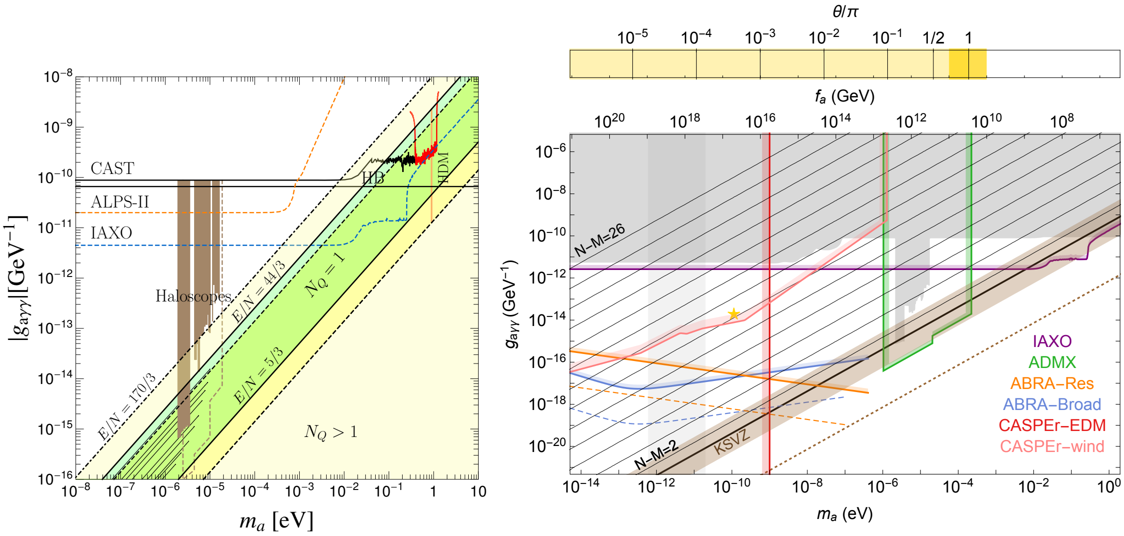

Figure 3.1: *Left:* The window for phenomenologically preferred hadronic axion models [?]. The green band encompasses models with a single R_Q. With more R_Q's the region below the line $E/N = 170/3$ becomes allowed. The two dashed lines enclose the usual window $|E/N - 1.92| \in [0.07, 7]$ [?]. Current (projected) exclusion limits are delimited by solid (dashed) lines. *Right:* The axion parameter space as a function of its mass m_a (and corresponding decay constant f_a) and its coupling to photons $g_{a\gamma\gamma} = \frac{c_\gamma}{f_a}\frac{\alpha}{2\pi}$ (figure from Ref. [?]). The colored lines represent the projected sensitivities of future experiments. In gray the region already excluded either by astrophysical observations or experiments as described in the text. The black solid line and brown band correspond to possible KSVZ QCD axion models. The thin lines illustrate the prediction of the clockwork QCD axion for $N - M = 2k$ with $k = 1, .., 13$ and with fermionic content as described in section 5 of Ref. [?]. In the upper band the figure shows the initial misalignment angle needed to reproduce the observed DM relic density. The darker yellow band corresponds to the uncertainty on f for the axion to be DM in the pre-inflationary axion scenario.

3.4 Search for Two-Photon Interaction with Axionlike Particles Using High-Repetition Pulsed Magnets and Synchrotron X Rays

New results of a search for two-photon interaction with ALPs were reported in Ref. [?]. The experiment was carried out at BL19LXU at the synchrotron radiation facility SPring-8. For this purpose, the experimental collaboration has developed a novel pulsed-magnet system, composed of multiple racetrack-magnets and a transportable power supply. It produces fields of about 10 T over 0.8 m with a high repetition rate of 0.2 Hz and yields a new method of probing the vacuum with high intensity fields. The data obtained with a total of 27,676 pulses provide a limit on the ALP-two-photon coupling constant that is more stringent by a factor of 5.2 compared to a previous x-ray LSW limit for the ALP mass $\lesssim 0.1$ eV, cf. Fig. 3.2 (right).

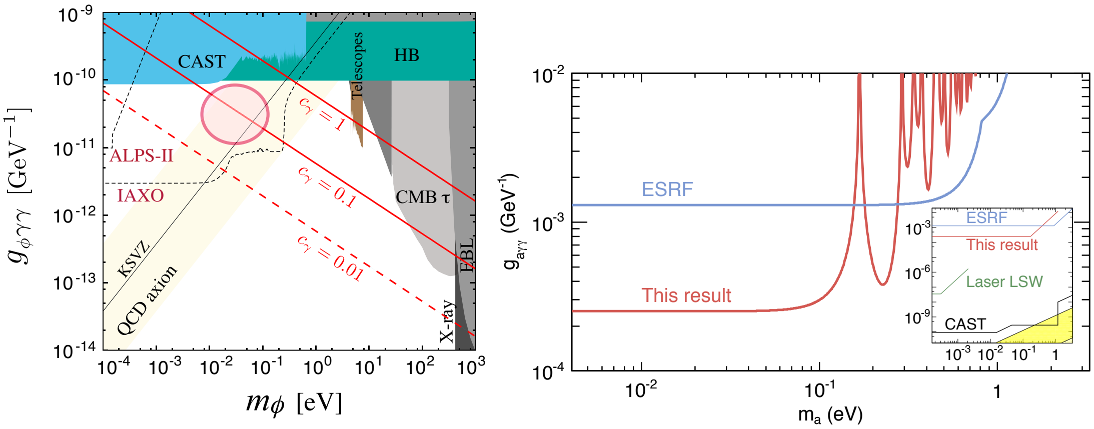

Figure 3.2: *Left:* The predicted relation between the ALP (inflaton) mass m_ϕ and the coupling to photons $g_{\phi\gamma\gamma}$ for $c_\gamma = 0.01, 0.1$, and 1 shown as red lines [?]. The dark shaded regions are excluded by various experiments and astrophysical/cosmological observaitons. For comparison, the predicted range for the QCD axion is shown as thin soild line and the light shaded region. The shaded circle represents a sweet spot region where the ALP miracle takes place. *Right:* Upper limit on the ALP-two-photon coupling constant $g_{a\gamma\gamma}$ at 95% C.L. as a function of the ALP mass from an LSW experiment exploiting synchrotron x-rays [?].

3.5 Dielectric Haloscopes: A New Way to Detect Axion Dark Matter

A new strategy to search for dark matter axions in the mass range of 40–400 μeV was proposed in Ref. [?] and its theoretical foundation was laid in Ref. [?]. It is based on the concept of dielectric haloscopes, which consist of dielectric disks placed in a magnetic field, cf. Fig. 3.3 (left). The changing dielectric media cause discontinuities in the axion-induced electric field, leading to the generation of propagating electromagnetic waves to satisfy the continuity requirements at the interfaces. Large-area disks with adjustable distances boost the microwave signal (10–100 GHz) to an observable level and allow one to scan over a broad axion mass range. A sensitivity to QCD axion models is conceivable with 80 disks of 1 m^2 area contained in a 10 Tesla field, cf. Fig. 3.3 (right).

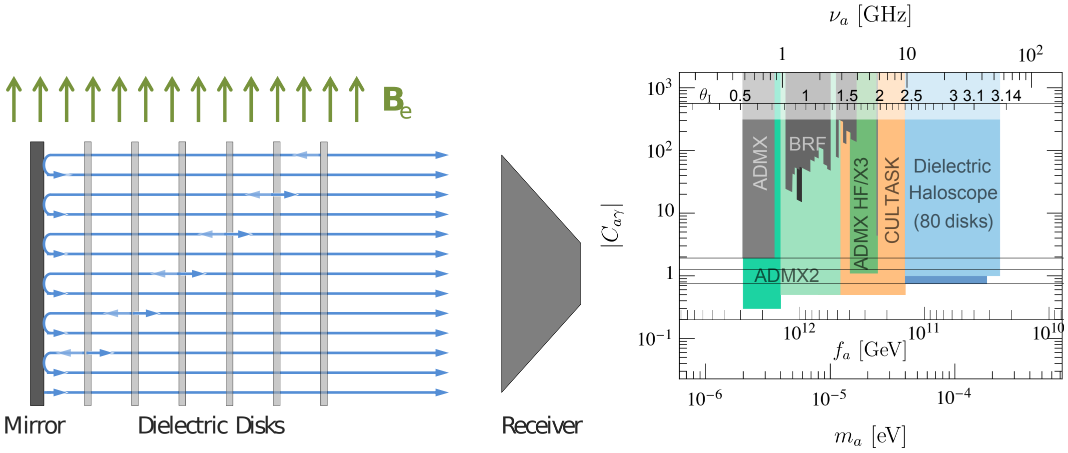

Figure 3.3: *Left:* A dielectric haloscope consisting of a mirror and several dielectric disks placed in an external magnetic field $\mathbf{B}_\mathrm{e}$ and a receiver in the field-free region [**?**]. A parabolic mirror (not shown) could be used to concentrate the emitted power into the receiver. Internal reflections are not shown. *Right:* Two examples of the discovery potential (light and dark blue) of our dielectric haloscope using 80 disks ($\epsilon = 25$, $A = 1\,\mathrm{m}^2$, $B_\mathrm{e} = 10\,\mathrm{T}$, $\eta = 0.8$, $t_\mathrm{R} = 1\,\mathrm{day}$) with quantum limited detection in a 3-year campaign [**?**].

4 Optics and related issues

A central breadboard was transferred from AEI Hannover to DESY, characterized and installed in the central tank. In addition to this, the regeneration cavity was locked by injecting a second infrared laser beam from the central table and the seismic noise as well as the optical losses were characterized.

4.1 Alignment of central breadboard

The central breadboard was fully assembled at AEI Hannover and transferred to DESY. Before the installation in the central vacuum tank a long term drift test of the angle between the flat mirrors defining the production and regeneration cavity eigenmodes was performed. The result is shown in fig. 4.1. Over the course of 187 h a drift of $1.7{\pm}0.26\,\mu$rad in the x direction and $2{\pm}0.32\,\mu$rad in the y direction is observed. This confirms previous measurements performed at AEI in Hannover and is within the ALPS requirements.

4.2 Improvement of frequency stabilization control loop

In previous experiments with the 20 m cavity the frequency stabilization control loop caused excess noise around the unity gain frequency due to a small phase margin. In order to address this problem we modified the control loop and shifted the pole frequency of the filter that is used to suppress the signal at twice the modulation frequency. Hence, we were able to recover 25 degree of phase margin at 55 kHz as depicted in fig 4.2.

4.3 Seismic noise projection

Figure 4.3 shows projections of the relative length noise of the regeneration cavity with and without the length control engaged along with the requirements for the length control. The dashed black line gives the half linewidth of the regeneration cavity for 532 nm light. The RMS of the regeneration cavity length noise with the length stabilization system engaged, must stay below this level for the system to remain stable. The solid black line is the dual resonance requirement for ALPS IIc which is one fifth the regeneration cavity half linewidth for 1064 nm light. The length noise of the regeneration cavity must be below this level with the passive filtering property of the cavity and the length stabilization engaged. This will ensure that the 95% of the light from the production cavity will couple to the regeneration cavity. The blue curve gives a measurement of the seismic noise in the ALPS IIa lab. A projection of the spectra of the regeneration cavity length noise with the length stabilization engaged is shown in green. Here we assume that the transfer function of the length control for the regeneration cavity has three integrators with a unity gain frequency of the 2.5 kHz.

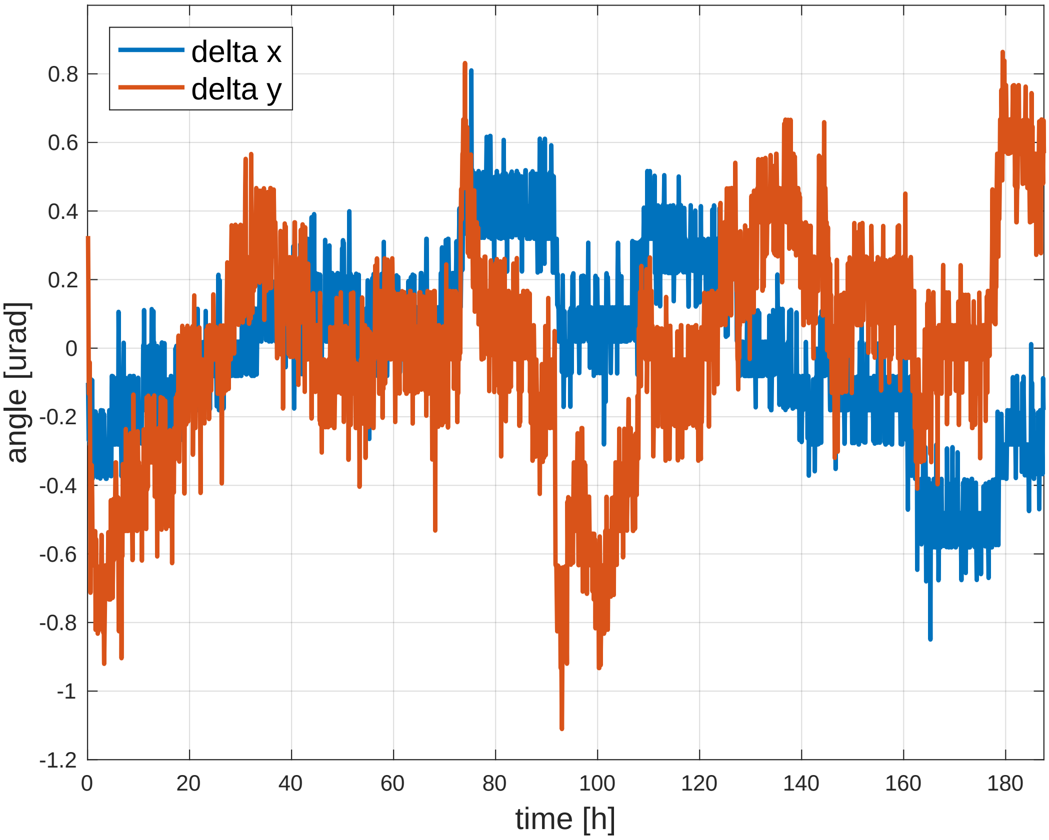

Figure 4.1: Relative drift measurement between the production and regeneration cavity end mirror. Over the course of 187 h the drift is 1.7 μrad in the x direction and 2 μrad in the y direction.

The dark red spectra shown in fig. 4.3 is the projected length noise of the regeneration cavity with respect to the production cavity circulating field filtered by the transfer function of the regeneration cavity for 1064 nm light. The RMS of this spectra, given by the dashed dark red line, must be suppressed below 0.2 pm for the regeneration cavity length stabilization system to meet the dual resonance requirements. In this case the total RMS for the filtered length noise is 0.19 pm. While the projection meets the requirements we have to demonstrate that we can build a length control loop according to these specifications with the new piezo actuator.

4.4 Regeneration Cavity

The current optical design of ALPS II contains a non-linear crystal on the central breadboard to generate the green light which is used to lock the regeneration cavity. This design has two major drawbacks. On the one hand the light transmitted from the production cavity needs to be aligned to the crystal in order to achieve optimum conversion efficiency. Hence, the production cavity eigenmode has to be aligned to a

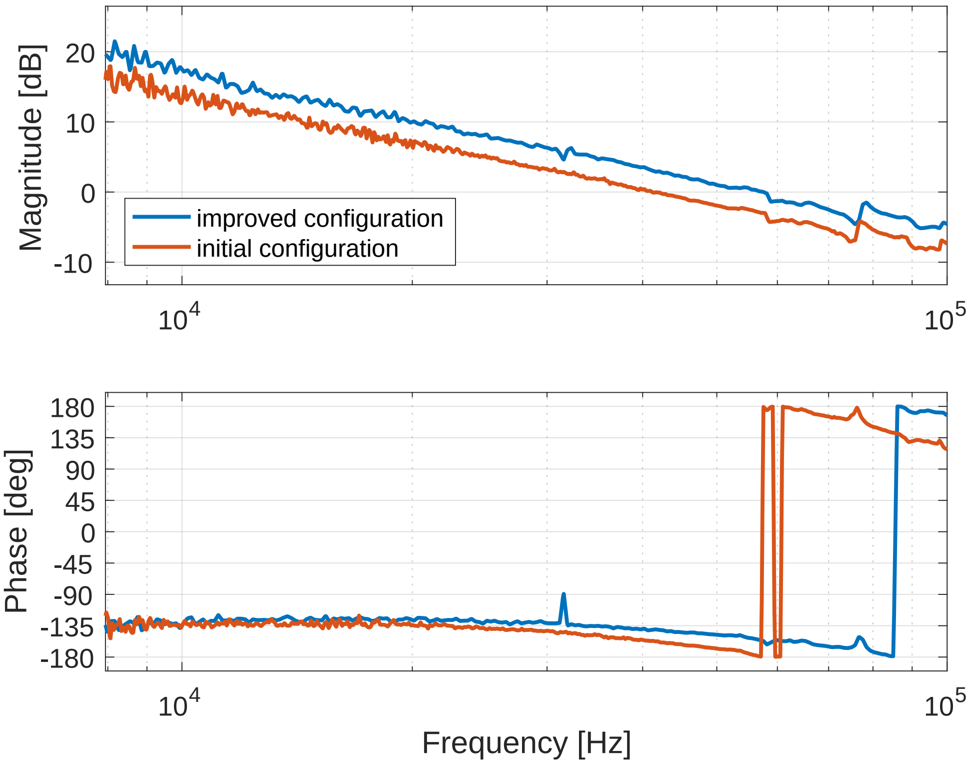

Figure 4.2: Transfer function measurement of the improved length control loop. Previously the loop lost 180 degree of phase margin at 55 kHz. The improved electronics phase loss at 55 kHz is only 155 degree. This allows for unity gain frequencies above 60 kHz.

certain spot on the end mirror and cannot be moved within the free aperture. On the other hand the second harmonic generation is a non-linear process and therefore the production cavity has to be operated with high circulating power in order to reach a sufficient output power for the green light. To circumvent these issues a new optics design is currently under discussion.

For first tests with the regeneration cavity we frequency locked a second NPRO[a] to the regeneration cavity to measure the losses from the mirrors and the power build-up for 1064 nm. On resonance with 50 mW incident on the regeneration cavity we saw 1.64 mW in transmission. The power transmissivity of the end mirror of the regeneration cavity is 2.5±0.3 ppm. On resonance 4.8 mW were reflected from the cavity yielding a mode matching of better than 98 %, a power buildup of 14000±3000, a circulating power of 660±80 W, and intra-cavity losses of 55±7 ppm. This is the lowest loss level we measured so far. However, to reach the design specifications we need to reduce additional losses by a factor of three.

In addition the frequency noise of the regeneration cavity was measured and compared to a previous measurements with the production cavity and a seismic noise projection

---

[a] This NPRO is located on the central table.

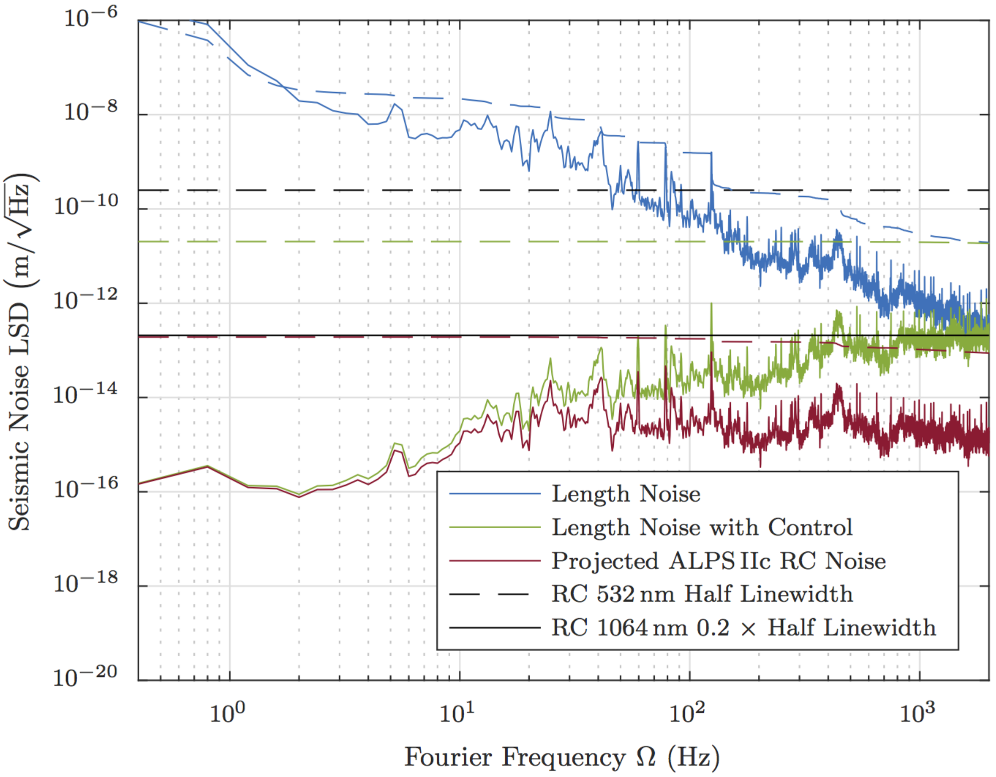

Figure 4.3: The blue curve is a measurement of the seismic noise in the ALPS IIa lab. The regeneration cavity relative length noise with the length stabilization system engaged is shown in green. A projection of the regeneration cavity length noise with the length stabilization and passive filtration by the regeneration cavity is shown in red. The integrated RMS for each of these spectra are given by their corresponding dashed lines. The dashed black line is the half linewidth of the regeneration cavity for 532 nm light. The solid black line is one fifth the regeneration cavity half linewidth for 1064 nm light.

as well as the typical NPRO frequency noise (see fig 4.4)[b]. The noise around the unity gain frequency of the regeneration cavity is elevated, since the control electronics are not modified and optimized yet. Excess frequency noise for the regeneration cavity between 10 Hz and 100 Hz is most likely due to a less robust mounting of the regeneration cavity end mirror. We are currently changing the design of this mirror mount to make it more stable and incorporate a faster piezo actuator.

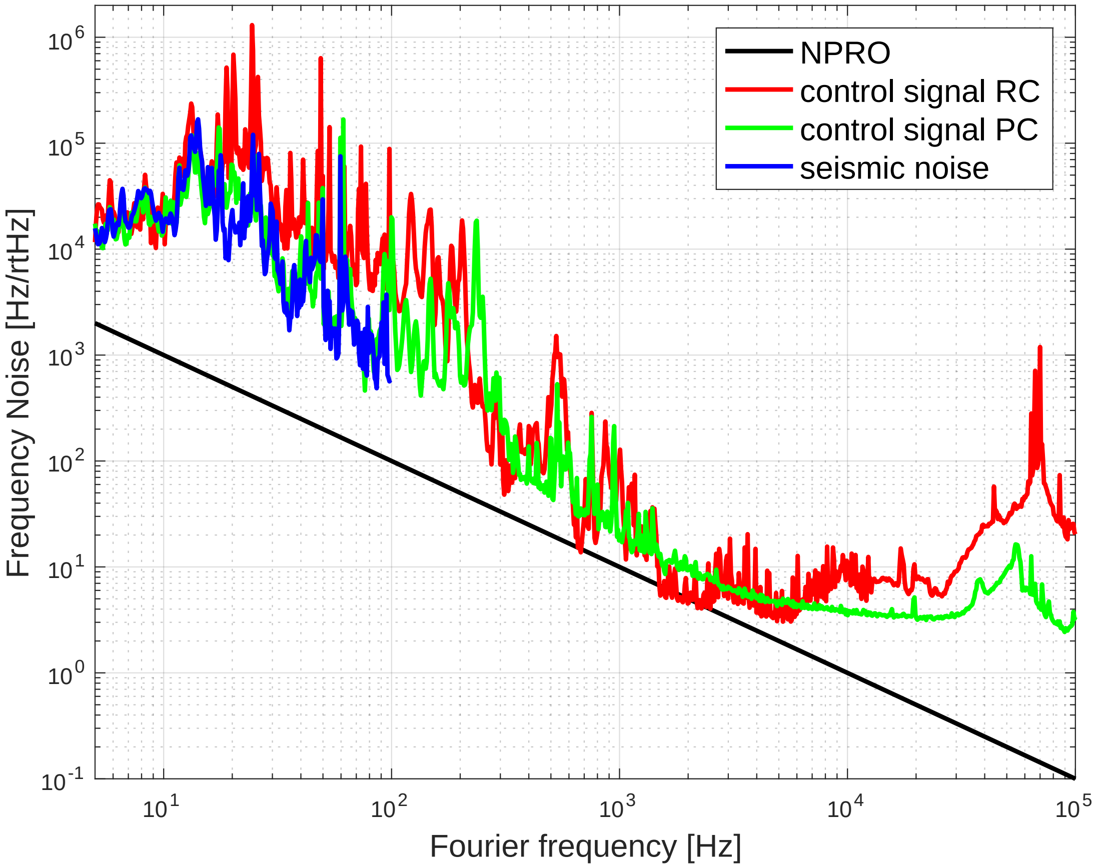

Figure 4.4: Measurement of the free running frequency noise (control signal) of production cavity and regeneration cavity as well as a frequency noise projection of the seismic noise.

4.5 Prospects

In the next months the optics activities will focus on the following items:

- discuss new optics design
- locking of regeneration cavity with green light and establish simultaneous resonance for green and infrared light

---

[b] The unity gain frequency is 35 kHz for the regeneration cavity and 55 kHz for the production cavity measurement.

- locking the regeneration cavity with feedback to the cavity length (new piezo actuator ordered for this test)
- check spatial overlap between production and regeneration cavity
- investigate thermal effects in the production cavity

5 Detector

In this chapter the status of the two detection schemes of ALPS II are presented. In the beginning the status of the single photon detection scheme, which is based on a *Transition Edge Sensor* (TES), is presented in Sect. 5.1. Following this, the status of the heterodyne detector system is presented in **??**.

5.1 TES detector system

5.1.1 ADR status

In the end of 2016 the ADR hold time at 80 mK was significantly reduced to about 20 min. In consequence, a photon detection was not possible any more, since the remaining time was not sufficient. Obviously, there was an additional heat flow from the 4K stage of the ADR to the salt pills. The salt pills unit was send to Entropy cryogenics in Munich for repair end of 2016. Following Prof. Dieter Horns, despite several attempts to fix the system malfunctions the suspension of the salt pills keeps ripping off during re-charges. Due to these problems with the salt pills and the ADR in general, Prof. Dieter Horns announced in November 2016 that he will leave the collaboration. In consequence, the ADR is no longer available to the ALPS collaboration and the TES cannot be operated anymore.

5.1.2 ADR replacement

We surveyed the market for available systems, that could be used as a replacement for the ADR system. In the end, it turned out that new dry dilution refrigerator systems are compatible to the ADR system with respect to the system size as well as the price. In addition, they can provide a higher cooling power compared to ADR systems. Moreover, they offer continuous operation at milli Kelvin temperature and no mechanical switches are operated at low temperature. Finally, no magnet is needed for the operation, which results in more space in the cryostat and no stray fields influencing the operation of the SQUIDs used to read out the TES signals. We already received DESY funds for a dry dilution refrigerator and we will start a tender as soon as possible. Considering the time needed for the tender process and typical delivery times a new system will not be available before October 2017.

5.1.3 Reduction of black body photon background events

Following the idea of filtering the black body photon background using a filter bench operated at cryogenic temperatures (70 K) presented in the 82$^{\text{nd}}$ PRC report, we set up such a filter bench at room temperature. A drawing of the filter bench including all components is shown in Fig. 5.1. In order to test the transmission for infrared light a

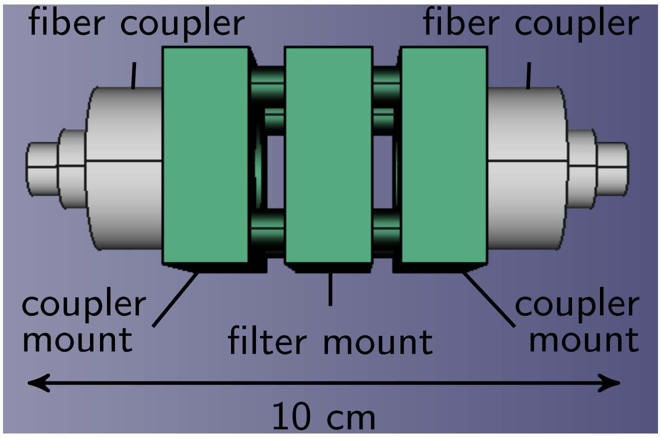

Figure 5.1: Drawing of the filter bench. All components are made of Titanium in order to guarantee a similar thermal expansion of the lenses/filter and the mountings.

fiber coupled laser was connected to one of the couplers mounted to the filter bench. A fiber coupled power meter was connected to the second coupler and at maximum a coupling efficiency from fiber to fiber via the filter bench of 82 % could be demonstrated at room temperature. Currently a beam splitter was added to the setup, which allows to monitor the laser power independently of the filter bench. This allows to decouple power fluctuations induced by the laser from coupling efficiency reductions due to a misalignment of the couplers of the filter bench. Since the ADR is no longer available we plan to cool the filter bench using dry ice (−80 °C) and test if the alignment is maintained. Up to this point standard optical fibers of type HI1060flex are used. In the final configuration bare fibers of the same type will be used in order to integrate them together with the filter bench inside the cryostat. Furthermore, the fiber tips will include an antireflective coating, which will increase the coupling efficiency per coupler. Assuming a loss due to reflections per fiber tip of 4 %, the coupling efficiency is expected to increase from 82 % to 89 % using antireflective coatings. If the test at −80 °C is successful we want to test the filter bench at 70 K in the final configuration.

5.1.4 Simulation of the black-body photons

The main dark count contribution for a fiber-coupled TES are thermal photons. There are two components from the black-body radiation: photons with an energy close to the signal photons and photons with smaller energy, which are arriving at the TES almost at the same time and produce pile-up events.

The spectrum of the black-body photons is described with Planck's law:

$$L(\epsilon, T) = \frac{2}{h^3 c^2} \frac{\epsilon^2}{e^{\epsilon/kT} - 1}, \tag{5.1}$$

where ϵ is the photon energy, T is the ambient temperature, k and h are Boltzmann and Plank constants and c is the speed of light.

However the spectrum of the black-body photons, which pass through the optical fibre and finally reach the TES, is different and depends on different fibre parameters. An

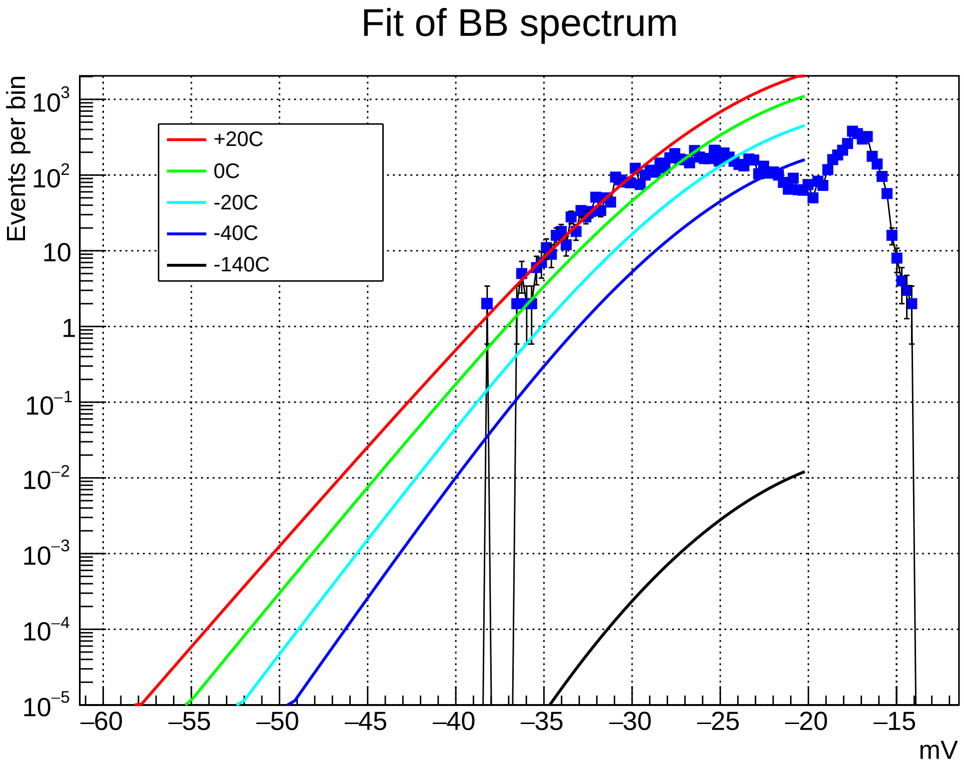

Figure 5.2: Pulse amplitude distribution from black-body photon events. The sample was recorded at cool-down 20 with a trigger threshold of -18.1 mV during 6 minutes.

example of a spectrum finally recorded with a fiber couled TES is shown in Fig. 5.2. During 6 minutes of data taken with a trigger threshold of -18.1 mV about 8.5×10^3 photon pulses have been recorded. Fig. 5.2 shows the pulse amplitude distribution of these pulses. The pulse amplitude depends linearly on the photon energy, where a pulse amplitude of -60 mV corresponds to a photon energy of about 1 eV.

The overall normalization of this spectrum depends on fibre properties (core diameter, numerical aperture). The distribution can be divided into the following regions:

1. The rapidly falling distribution in the region -18 to -14 mV is determined by the trigger efficiency.

2. The exponentially rising spectrum in the region -20 to -18 mV is an effect of electrical noise in the output voltage.

3. The region -30 to -20 mV is determined by black-body photons and suppressed by the fibre transmittance. This suppression depends on fibre type, length of the fibre and actual shape of the fibre (radius of curvature, number of loops).

4. The region -40 to -30 mV is well described with Planck's function at 20 °C (lab temperature) convoluted with a Gaussian resolution of 5 mV (The TES energy resolution is known from studies of the noise in the output signal). This region is not affected by a reduced fibre transmittance due to higher photon energies.

The fit of Planck's function convoluted with a Gaussian energy resolution is shown as red line in Fig. 5.2 and extrapolated over a wider photon energy range. The only free parameter in the fit is the overall normalization, while other parameters were fixed to known values. Our data are very well reproduced by the fit.

An effect of changing ambient temperature to the spectrum is demonstrated by considering the same function, which was used for the fit, at different temperatures. The effect is mostly uniform over the wide energy range. Taking into account the idea of installing a filter bench operated at 70 K (see Sect. 5.1.3) one can estimate the improvement in terms of background rate. Even going to −140 °C reduces the number of events by five orders of magnitude. Pile-up events are reduced further in case of the filter bench by the band-pass filter installed in the bench.

In order to study black-body photons in more detail a Monte-Carlo event by event simulation technique has been used. Each event in this simulation contains 500 data samples taken with a sampling rate of 20 MSPS. In other words an event is a time line with a length of 25 µs. The pulse shape was simulated according to small signal theory and the noise added in the simulation was deduced from real data time lines. The pulse amplitude is sampled from the black-body spectrum described above.

Black-body photon events are characterised by a single pulse, originated from a black-body photon with an energy near by the energy of signal photons (about 1 eV). Since the spectrum of the black-body photons exponentially drops with increasing energy most of the events include pulses with an amplitude close or even below the trigger threshold. In the latter case, the trigger fired because of the electronic noise is added on top of the simulated pulse and the pulse amplitude is increased just above the threshold.

The exponential behaviour results in the fact that most of the black-body photon background events will be on the low energy side of the signal region. A lot of photons with energy below the energy of signal photon will enter signal region just because of noise fluctuations. If a narrow band-pass filter is used in the filter bench many of these events could be reduced. This effect was studied in a simulation and the results is shown in Fig. 5.2. Here the signal region is assumed to be around −67 mV. The considered photon energy for events simulated without the filter (black distribution) corresponds to a voltage range of −80 to −55 mV. This range covers all photons that could end up in the signal region due to noise fluctuations. The red distribution includes events as expected when a narrow high-pass filter is used. The filter cut-off corresponds to a voltage of −65 mV. In consequence, the voltage range covered by events corresponding to the red distribution is −80 to −65 mV. The suppression achieved using the filter is up to one order of magnitude.

Considering pile-up events one can argue that they require at least two photons which results in a quadratic suppression compared to the suppressing of the total black-body photon rate described above. Therefore, e.g. lowering the temperature to −40 °C (or installing the filter at this temperature) would reduce the black-body photon rate by at least one order of magnitude (see Fig. 5.3) and reduce the pile-up rate by more then 2 orders of magnitude.

In summary, we are very confident to be able to suppress the black body photon induced background on the TES by many orders of magnitude with the help of a filter bench at cryogenic temperatures. We expect to reach a background rate of $10^{-}4$ counts per second also with installed fibers and without the necessity to cut away 50% of the

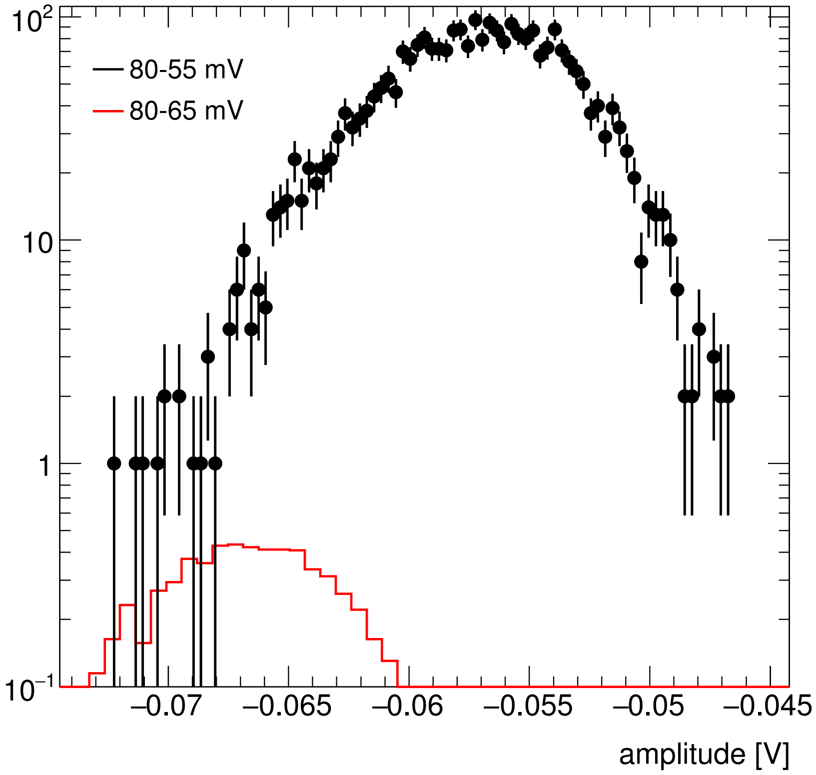

Figure 5.3: A comparison of distributions of the reconstructed pulse-amplitudes of two simulated samples of the black-body photon events. The black distribution corresponds to non-filtered events, while the red distribution represents high-pass filtered events with a filter cut-off corresponding to $-65\,\text{mV}$. The signal region is assumed to be around $-65\,\text{mV}$, where the filtered sample demonstrates about 1 order of magnitude suppression.

signal region (the low energy part).

5.2 Heterodyne Axion detection scheme

In the ALPS experiment, the detectable signal is that of regenerated photons at a very specific, known frequency. Due to the low probability conversion/reconversion of photons and axions the amplitude of the signal field is on the order of 1 photon / 2 weeks. By overlapping the signal with a strong local oscillator field (see Figure 5.4) at a slightly different frequency, the interference between the two beams will create an observable beat note in the RF band. Amplitude and phase information of the signal can be obtained from this beat note via demodulation techniques.

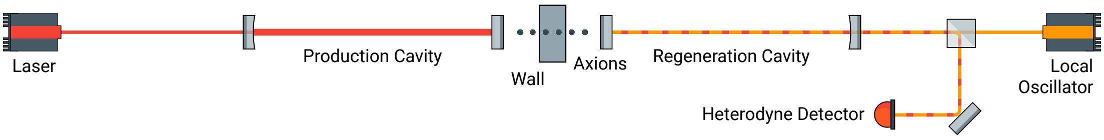

Figure 5.4: Simplified layout of the ALPS experiment. The regenerated photons are overlapped with a local oscillator field and the beat note is obtained via a photodetector.

5.2.1 Basic principle

The photodetector signal is digitized via an Analog-to-Digital convertor onboard a Field Programmable Gate Array (FPGA) card. As the frequency of the RF signal is known, by multiplying the ADC input with a sine/cosine at the same frequency, f, and digital low pass filtering, amplitude information can be obtained.

$$I = A\sin\left(ft+\phi\right) \times \cos\left(ft\right) = \frac{A}{2}\left[\sin\left(\phi\right)\right] \tag{5.2}$$

$$Q = A\cos\left(ft+\phi\right) \times \sin\left(ft\right) = \frac{A}{2}\left[\cos\left(\phi\right)\right] \tag{5.3}$$

Even with an unknown phase, retaining both I and Q data and summing them in quadrature allows for amplitude measurements. When the regenerated photons are coherent with the local oscillator, the signal will integrate up over time where as incoherent noise will not. It can be shown that for N samples, with noise having variance σ and mean $\langle\zeta\rangle$

$$\frac{\sqrt{\left(\sum_{n=1}^{N} I\right)^2 + \left(\sum_{n=1}^{N} Q\right)^2}}{\sqrt{N}} \longrightarrow \sqrt{\frac{A^2}{4}N + \frac{A^2}{4} + \sigma + \langle\zeta\rangle} \quad . \tag{5.4}$$

When only noise is input in the system (A=0) a plot of the Left Hand Side (LHS) vs. N will stay flat. When a signal is present, for small A and N the curve will behave as if only noise is present. Once N becomes large enough, the signal will peak out of the noise and increase as $\sqrt{N}$. This has been shown to be true in both simulations and preliminary results, shown in Fig. 5.5.

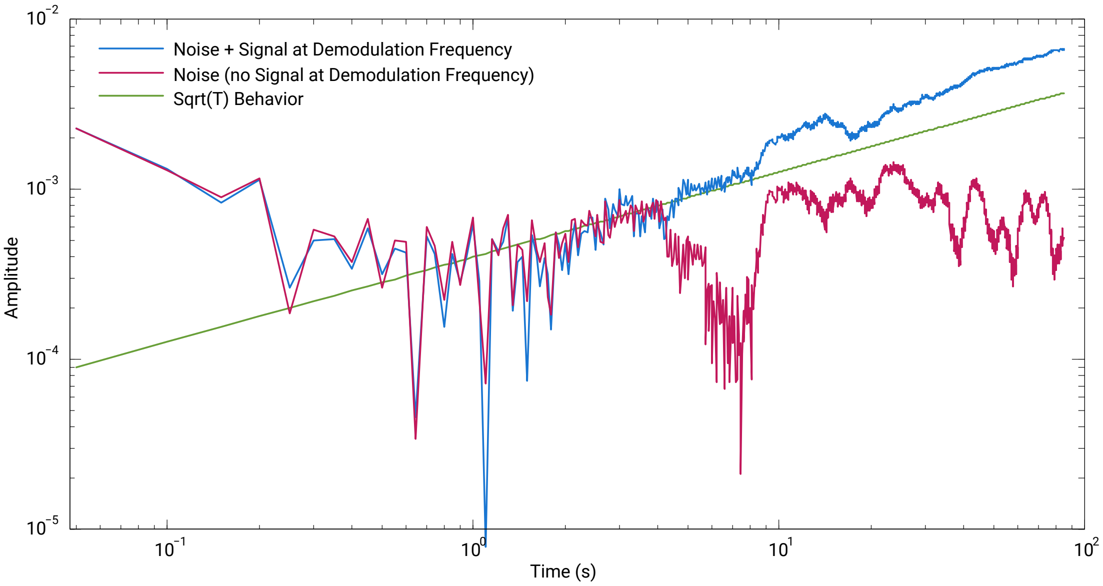

Figure 5.5: Amplitude $\sqrt{(\Sigma I)^2 + (\Sigma Q)^2}/\sqrt{N}$ over time for electrical signal with gaussian noise and random frequency components at different amplitudes. In blue: Phase coherent signal injected at the demodulation frequency. In red: Phase coherent signal present, but at frequency different from demodulation frequency. in green: expected behaviour for a phase coherent signal at the demodulation frequency (offset depends on signal amplitude).

5.2.2 Double demodulation

We at the University of Florida have constructed this setup and are currently taking data for preliminary results with real signals. For this process to work the demodulation process must be done in two parts. This is due to the sensitive nature of the FPGA to internal signals of the desktop computer. Signals coherent with the clock generator are picked up by the card and are always mixed down the DC levels. If a single demodulation stage is done using only the FPGA, mixing the RF signal down to DC will be overshadowed by the spurious signal present. To correct for this, the RF signal is mixed down on the FPGA (see Fig. 5.6) to a frequency close to DC. This is done by multiplying the ADC by sine at a slight offset ϵ from the signal frequency f_{s} (demodulation frequency $f_{\mathrm{s}} + \epsilon$).

This data is then stored to a buffer where it is saved to file via LabView (see Fig. 5.7). The FPGA operates at 64 MHz and is downsampled via CIC filters to 31.25 kHz before being stored to the buffer. LabView reads the buffer in packets of 1562 samples. Each packet is summed and the summed value is written to file. This causes the write speed to be 31.25 kHz / 1562 or approximately 20 Hz. The saved data is then imported into MatLab where the multiplication by cosine/sine at frequency ϵ is done to shift the real signal to DC and the spurious signals to a non-zero frequency where they will be integrated away. The signal input into the ADC was at 16 MHz + 7 Hz. The FPGA mixes this data with a sine at 16 MHz. The peak at DC is the spurious signal while the peak at 7 Hz is the signal of interest. By multiplying this by cosine/sine at 7 Hz for the example above, the spurious signal will shift to a nonzero frequency and the signal of interest will go to DC.

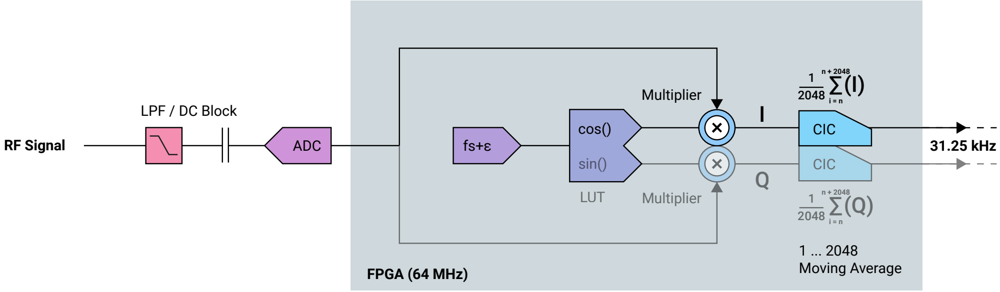

Figure 5.6: An RF signal at frequency f_s is digitized by the ADC onboard the FPGA card operating at 64 MHz. It is then multiplied by the output of of a Look Up Table (LUT) which generates a sine waveform at $f_s + \epsilon$. This shifts the signal of interest down to ϵ. A moving average CIC filter decimates the data down to 31.25 kHz where it can be stored to a buffer.

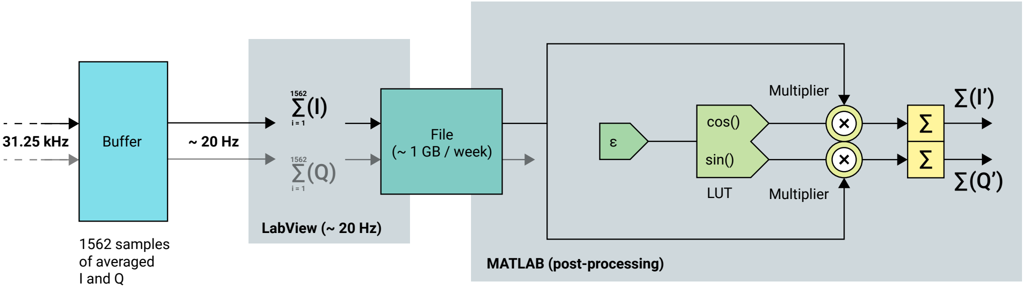

Figure 5.7: The stored data on the buffer is read via DMA transfer using LabView software. LabView reads the buffer in packets of 1562. A second moving-sum filter is used to once again downsample the data now to approximately 20 Hz. This data is then stored as a raw .txt file on the desktop computer. The data is imported into MatLab and is demodulated a final time. Using a LUT in MatLab to generate at sine/cosine at ϵ to generate the I/Q data respectively. In this step, the signal is shifted to DC, while the spurious signal moves to a non-zero frequency, where it will integrate away. Finally, the I/Q data is summed individually such that $\sqrt{(\Sigma I)^2 + (\Sigma Q)^2}/\sqrt{N}$ can be computed.

SIGvNOISE

5.2.3 Application

This double demodulation technique was tested using a function generator synchronized to the clock of the FPGA card. The input signal strength can be adjusted using a function generator. Results of this test are shown in Fig. 5.8.

As expected, with the function generator turned off (red curve) the response is flat as total number of samples N increases. However, with an antenna at a specified frequency, the signal slowly integrates up above the noise level, and continues to grow as square root of N. If we shorten the cable of the antenna, this reduces the amplitude of the signal and requires more samples for it to peak out of the noise. Data runs are limited to approximately 7 hours before LabView runs out of memory; however, improvements to the code are currently being implemented to allow for longer data collection time.

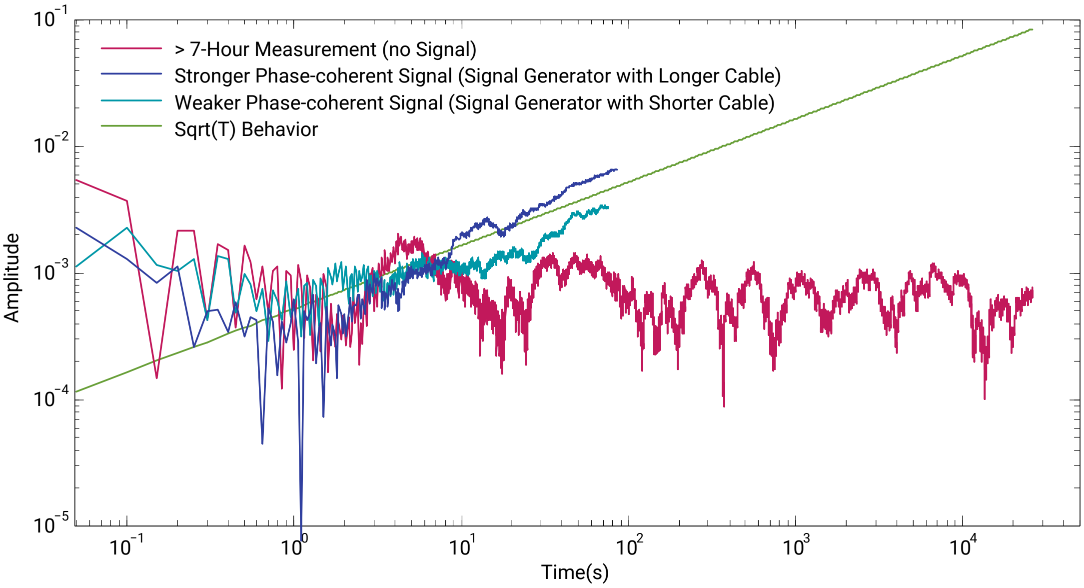

Figure 5.8: Plot of $\sqrt{(\Sigma I)^2 + (\Sigma Q)^2}/\sqrt{N}$ vs time. Time can be plotted on the x-axis because it is proportional to sample number. The red curve corresponds to no signal at the input (noise only). When a signal is present at the input, the curves increase as $\sqrt{t}$ (green curve). However, for a stronger signal as shown in the blue curve, the signal peaks out of the noise earlier than a weaker signal, as shown in the green-blue curve.

6 Data acquisition and slow control system

In the following, work related to the ALPS II control and data acquisition system is summarized. Mainly, we put effort into developing a common software framework for ALPS II, that covers a common data format, data acquisition software and analysis tools. Furthermore, different ADC options were characterised with respect to their noise levels. Finally, the DOOCS[c] based control system was improved and extended.

6.1 Control signal monitoring

In the following two different ADC options are discussed that will be used to monitor cavity related control signals. Basically, there are two different use cases, each with different requirements.

1. Fast sampling of photodiode signals for a limited time period, that allows to characterise system noise and is used mainly in the commissioning phase of ALPS II.
2. Long term sampling of photodiode signals used to monitor for example the cavities status (locked or not locked) or the power build up in the cavities.

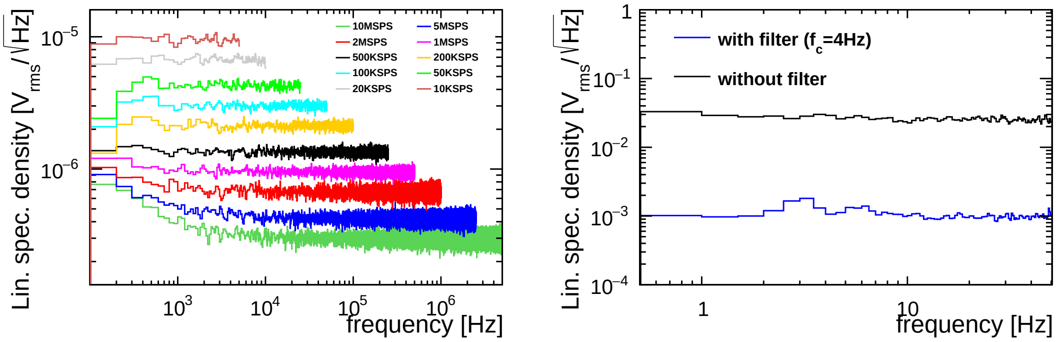

(a) ALAZAR ATS9416 for different sampling rates without anti-aliasing filter.

(b) MCP3204 chip with and without anti-aliasing filter operated at 100 SPS sampling rate.

Figure 6.1: Linear spectral density acquired with two different ADC options. In both cases the input port was terminated with a 50 Ω resistor.

---

[c] Distributed Object Oriented Control System

6.1.1 Fast monitoring system

For the fast monitoring of photodiode signals a 16 channels ADC board[d] offering a 14 bit resolution for a fixed voltage range of ±1 V was set up. Its maximum sampling rate is 100 MS/s and up to 4 GS can be stored in the onboard memory. Furthermore, the board features the possibility to write directly to the memory of the host system. This technique is called DMA (direct memory access) and was already discussed in the 81st PRC report by taking the example of the ALAZAR card used to read TES signals. The transfer speed was proven to be 3.5 GB/s. The linear spectral density without an anti-aliasing filter is shown in Fig. 6.1a for one channel. The noise level shown in Fig. 6.1a needs to be known in order to design the amplifier used later on to amplify the photodiode signals.

Currently we design an anti-aliasing filter that is required for spectral noise studies with the ADC board. The anti-aliasing filter and a gain stage for all 16 channels will be integrated on a dedicated board that will be directly connected to the ALAZAR board.

6.1.2 Long term monitoring system

For the long term monitoring system we tested a 4 channel ADC[e] featuring 12 bit resolution. This ADC can directly be interfaced with a Raspberry Pi[f]. The maximum sampling rate is 100 kSPS, but we intent to operate it at a sampling rate of 10 SPS, which is sufficient to monitor cavity parameters like the power build up. We successfully tested this ADC at 100 SPS controlling it with DOOCS[g]. The spectral noise density resulting from the test is shown in Fig. 6.1b. Again, in order to do a spectral noise analysis an anti-aliasing filter needs to be implemented. So far we used a 1st-order low pass filter with a cut-off frequency of $f_c = 4\,\mathrm{Hz}$. Results including this filter are also shown in Fig. 6.1b. As can be seen the anit-aliasing filter reduced the noise floor by more than one order of magnitude.

Next, we will integrate one anti-aliasing filters and one voltage converter stage per channel for four channels on a single board. The voltage converter stage is needed to translate the signal to be measured (-15 to 15 V) to a range that can be handled by the ADC (0 to 5 V). It was already included in the ADC test presented above.

6.2 Software framework

The current framework contains three main packages:

alpsIO: Handling of acquired and simulated data.

alazar: Data taking with ALAZAR boards used by the TES data acquisition system and the fast monitoring discussed above.

analysis: TES data simulation, TES data analysis, time line analysis.

---

[d] ALAZAR ATS9416

[e] Microchip MCP3204

[f] Small single-board computer developed by the Raspberry Pi Foundation

[g] 100 Hz is the maximum update frequency in DOOCS

The framework makes use of object oriented programming and is written in C++. Furthermore, the ROOT[h] software framework is used at different stages. Details about the packages are given in the following.

6.2.1 alpsIO package

This package is used to handle data related to the ALPS II experiment. Currently three data formats are supported:

- ASCII files
- Binary files
- ROOT files

The support for ASCII files allows to read TES data that were taken with an oscilloscope[i] in the past. In future we will use an ALAZAR board to acquire TES data (see 81st PRC report). Here the preferred data format will be ROOT files, since ROOT offers a loss less data compression. For the fast control signal monitoring discussed in Sect. 6.1.1 writing of compressed ROOT files will not be possible, because data needs to be written as fast as possible to disk in order to free RAM memory during the data acquisition. Here binary files or uncompressed ROOT files will be used.

A major improvement of the alpsIO package implemented recently is the option to write raw data in units of ADC counts rather than writing converted data in units of volts. In terms of data size this means writing 2 byte per sample for the raw data instead of 8 byte for the converted data sample. In consequence the data size was reduced by a factor of 4. The size of the compressed ROOT files was reduced by a factor of 2 when writing raw data instead of converted data.

6.2.2 alazar package

This package allows to acquire data with readout boards of the company Alazar Technologies Inc.[j]. It is based on the software development kit provided by Alazar Technologies Inc.. The package allows to acquire data using different schemes as discussed in PRC reports 81 and 82. As discussed in the previous section a major change of the packages is new option to acquire raw data instead of converted data. Furthermore, the package was written in a more generic way allowing for example to take data for 16 channels rather than just for two channels. This change was introduced to utilize the new ALAZAR board introduced in Sect. 6.1.1.

6.2.3 analysis package

The analysis package currently covers the TES signal simulation, TES data analysis and the analysis of time lines. The latter one is used to analyse control signals of the optics system with respect to spectral density noise as shown e.g. in Fig. 6.1. In detail a *Fast*

---

[h] An object oriented framework for large scale data analysis developed at CERN.

[i] Tektronix DPO7104C

[j] Alazar Technologies Inc., Suite 310 Pointe-Claire, QC Canada H9R 4S2

Fourier Transformation (FFT) is performed. In addition, several window functions can be applied to the time line to artificially generate a periodic signal and avoid artifacts in the FFT result. When specifying a certain frequency resolution, the time line is automatically split into sub samples. The FFT is performed on each sub sample and the result is an average over all sub samples per frequency bin. Here the arithmetic average or the median can be chosen.

The simulation of TES pulses is based on the ideal pulse shape described by the small signal theory [**?**]. Additional noise can be added to the pulse, by providing a linear spectral density. If using the linear spectral density resulting from TES background measurements this already accounts for the bandwidth of the SQUID stage. Finally, one ends up with a realistic simulated data sample. On the TES data analysis side, the pulse finding and fitting is included in the analysis package. An application of this package can be found in Sect. 5.1.4.

6.3 ALPS control system

Our DOOCS based control system was extended by one server that allows to control and read two types of ADCs – the MCP3204 chip introduced in Sect. 6.1.2 and ADCs that are onboard of an Arduino Uno microcontroller. In detail, there are 6 ADCs on the Arduino, which provide 10 bit resolution. A control panel was created in order monitor and control the ADCs via the DOOCS server. A screen shot of that panel is shown in Fig. 6.2. In the upper left part of the panel the reference voltage used to convert ADC units to voltage and the sampling rate can be set. In the bottom left part the latest ADC values read from the DOOCS server are shown including the converted data. These data is shown using dynamic lists. This means that the number of channels is not fixed in the panel, but it is read from the DOOCS server and the list is filled accordingly. This allows to use the same panel for both the MCP3204 chip and the Arduino microcontroller. The user can choose the device to be read using the device chooser in the top center part of the panel. For the conversion from ADU units to voltage also the resolution is read dynamically from the server. In the right part of the panel the history of each ADC channel value in ADC units is shown.

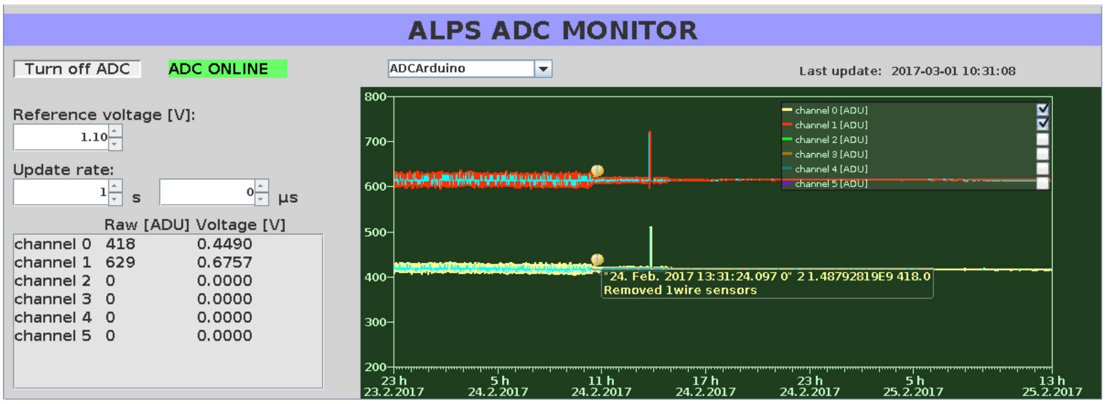

ADCArduino

Last update: 2017-03-01 10:31:08

Reference voltage [V]: 1.10

Update rate: 1 s 0 µs

	Raw [ADU]	Voltage [V]
channel 0	418	0.4490
channel 1	629	0.6757
channel 2	0	0.0000
channel 3	0	0.0000
channel 4	0	0.0000
channel 5	0	0.0000

"24. Feb. 2017 13:31:24.097 0" 2 1.48792819E9 418.0
Removed 1wire sensors

Figure 6.2: Control panel for the MCP3204 ADC and the onboard ADCs of an Arduino Uno. The screenshot illustrates the dynamic list of channels, a histogram of the ADC value per channel and the controls to change the sampling rate and the reference voltage used to convert ADC values to voltage values. Furthermore, the feature of tool tips is illustrates in case of a message from the operator that is stored in the history: “Removed 1wire sensors.”. The blue line added to each data line in the histogram indicates the time averaged data trend.

7 HERA dipole magnets

Since the successful test of the straightened HERA dipole BRp 212 with quench currents of $\sim 6500\ A$, reported to the last PRC meeting in October 2016, no further dipole has been mounted onto the test bench. The manpower required for the continuation of the straightening of dipoles was busy with the completion of the European XFEL.

Before the next dipole can be operated on the test bench, the overpressure valves in the cryogenics system of the test bench have to be checked according to safety regulations. The preparation for these tests has started.

The installation of the next HERA dipole on the test bench is planned for March 2017.

The schedule for the straightening, the removal of accelerator components in the straight section HERA North, and the installation of the dipoles for ALPS IIc is being discussed with DESY groups involved in the work. The special transportation vehicle (HERA tram), needed for the removal of the larger accelerator components, is being overhauled at present and should be available in April 2017.

8 Collaboration issues

The collaboration has faced some changes in the past six months:

- Noemie Bastidon (University of Hamburg) finished her Ph.D. thesis on the Transition Edge Sensor detector system.
- Christoph Weinsheimer (University of Mainz) will finish his Ph.D. thesis on the TES detector system and the ALPS DAQ soon.
- Nataliia Kuzkova (DESY) decided to not finish her Ph.D. thesis at ALPS but moved to Berlin due to personal circumstances.
- Dieter Horns (University of Hamburg) decided to leave the ALPS II collaboration at the end of the year 2016.

The present composition of the ALPS collaboration is depicted in Tab. 8.1. Discussions are ongoing with new potential ALPS II partners. Some details might be presented at the next PRC meeting. In late April 2017 a new DESY optics Ph.D. student will start working with ALPS II.

Institute	**Topics**	**Staff scient.**	**Engineers**	**P.docs**	**Stud.**
DESY	optics, detector, magnets, infrastructure	2 (part time)	1 (part time)	3	1
AEI	optics	1 (part time)		1	2
Hamburg University	optics			1	
Mainz University	detector	1 (part time)			(1)
University of Florida	optics, infrastructure	2 (part time)	1 (part time)	1	2

Table 8.1: The ALPS II collaboration as end of February 2017. In addition, D. Trines (retired) takes care for the HERA dipole magnet straightening and the organization of the work in the HERA tunnel towards ALPS IIc.

In the year 2016 ALPS collaboration members have, among others, contributed to the following WISP physics related publications and proceedings as given in the bibliography: [?], [?] [?, ?, ?, ?, ?, ?, ?, ?, ?] They have given the presentations and invited talks related to ALPS II as listed below.

- “The Hunt for ALPs" (A. Ringwald), Particle and Fields Seminar, University of Oxford, United Kingdom, February 2016

- “Light shining through wall experiments” (J. H. Poeld), Bethe Forum: Axions and the low energy frontier, Bonn, March 2016
- “The ALPS II experiment” (A. Lindner), IAXO workshop, INFN Frascati, Italy, April 2016
- “Status of the ALPS II experiment” (J. H. Poeld), PRC81 open session, DESY, Hamburg, April 2016
- “ALPs: Experimental landscape” (A. Lindner), IAXO in Germany, DESY, May 2016
- “Axions and ALPs” (A. Ringwald), IAXO in Germany, DESY, May 2016
- “Illuminating the dark side: new approaches to search for the dominating matter in our universe” (A. Lindner), Physics Colloquium, University of Wuppertal, May 2016
- “SM*A*S*H” (A. Ringwald), Theoretical HEP Seminar, Technical University of Munich, June 2016
- “SM*A*S*H - Standard Model * Axion * See-saw * Hidden scalar inflation” (A. Ringwald), 12th Patras Workshop on Axions, WIMPs and WISPs, Jeju Island/South Korea, June 2016
- “SM*A*S*H - Standard Model * Axion * See-saw * Hidden scalar inflation” (A. Ringwald), From the Vacuum to the Universe, Kitzbühel, Austria, June 2016
- “Illuminating the dark side: new approaches to search for the dominating matter in our universe” (A. Lindner), Research Training Group seminar, University of Jena, July 2016
- “Illuminating the dark side: new approaches to search for the dominating matter in our universe” (A. Lindner), Research Training Group seminar, RWTH Aachen, July 2016
- “Status of ALPS II” (M. Karnevskiy), Identification of Dark Matter 2016, Sheffield, United Kingdom, July 2016
- “Physics Case for Axion or ALP Dark Matter” (A. Ringwald), Identification of Dark Matter 2016, Sheffield, United Kingdom, July 2016
- “Future options for searching axion-like particles through light-shining-through-a-wall experiments” (A. Lindner), Physics beyond colliders, CERN, Switzerland, September 2016
- “Axion and Axion-Like Particles: Physics Case for Experiments” (A. Ringwald), Physics beyond colliders, CERN, Switzerland, September 2016
- “Alternative Dark Matter Candidates: Axions” (A. Ringwald), NOW 2016, Otranto, Italy, September 2016

- “Axion physics: solving enigmas of elementary particle physics and of the cosmos?” (A. Lindner), Colloquium NIKHEF, Amsterdam, Netherlands, October 2016
- “Path towards ALPS II and beyond” (J. H. Poeld), NIKHEF, Amsterdam, Netherlands, October 2016
- “A Minimal Model for Particle Physics and Cosmology” (A. Ringwald), 8th Bethe Center Workshop, Physikzentrum Bad Honnef, October 2016
- “Topology in QCD and Axion Dark Matter” (A. Ringwald), Symposium on Advances in Semi-Classical Methods in Mathematics and Physics, Groningen, The Netherlands, October 2016
- “Axion physics: solving enigmas of elementary particle physics and of the cosmos?” (A. Lindner), Physics Colloquium, University of Bonn, November 2016
- “SM*A*S*H – A Minimal Model for Particle Physics and Cosmology” (A. Ringwald), Theory Colloquium, DESY, Hamburg, November 2016
- “SM*A*S*H – A Minimal Model for Particle Physics and Cosmology” (A. Ringwald), Dark Matter from aeV to ZeV, Lumbley Castle, United Kingdom, November 2016
- “ALPS II at DESY and prospects for future light-shining-through-a-wall experiments” (A. Lindner), Axion dark matter at Nordita, Stockholm, Sweden, December 2016
- “Axion Cold Dark Matter” (A. Ringwald), Axion dark matter at Nordita, Stockholm, Sweden, December 2016
- “SM*A*S*H – A Minimal Model for Particle Physics and Cosmology” (A. Ringwald), Axion dark matter at Nordita, Stockholm, Sweden, December 2016
- “The Quest for Axions and Axion-Like Particles” (A. Ringwald), Hidden Sector and Cosmophysics, Kyoto, Japan, December 2016

9 Towards an ALPS IIc project

A detailed plan for the work in the HERA tunnel and hall has been drafted and is discussed at present with the technical infrastructure groups. The refurbishment of the HERA tram necessary to move heavy equipment in the HERA tunnel has started. It is expected to have the tram operational again in April. Then the clearing of the HERA tunnel for ALPS IIc will begin. Some resource issues have come up, because in-house personal previously meant to work in HERA for ALPS IIc is not available any more so that the ALPS project has to find money to hire external people.

The magnet straightening is on the critical path at present.

The Work Breakdown Structure (WBS) of the ALPS IIc project will be finalized at the next ALPS II collaboration meeting in March 2017. For ALPS IIc we presently discuss a revised optics concept from lessons learned at ALPS IIa. It should also allow for comparable simple switching between the TES detector and the heterodyne detection scheme. We hope to be able to sketch this new scheme at the forthcoming PRC meeting.